Glass Transitions, Semiconductor-Metal Transitions, and Fragilities in Ge-*V*-Te (*V* = As, Sb) Liquid Alloys: The Difference One Element Can Make

Shuai Wei,[1,2] Garrett J. Coleman,[2] Pierre Lucas,[2] and C. Austen Angell[1,*]
[1]*School of Molecular Sciences, Arizona State University, Tempe, Arizona 85287-1604, USA*
[2]*Department of Materials Science and Engineering, University of Arizona, Tucson, Arizona 85721, USA*

(Received 25 October 2016; revised manuscript received 5 February 2017; published 31 March 2017; corrected 25 September 2017)

Glass-transition temperatures (T_g) and liquid fragilities are measured along a line of constant Ge content in the system Ge-As-Te, and contrasted with the lack of glass-forming ability in the twin system Ge-Sb-Te at the same Ge content. The one composition established as free of crystal contamination in the latter system shows a behavior opposite to that of a more covalent system. The comparison of T_g vs bond density in the three systems Ge-As-chalcogen differing in chalcogen, i.e., S, Se, or Te, shows that as the chalcogen becomes more metallic, i.e., in the order S < Se < Te, the bond-density effect on T_g becomes systematically weaker, with a crossover at $\langle r \rangle = 2.3$. When the more metallic Sb replaces As at $\langle r \rangle$ greater than 2.3, incipient metallicity rather than directional bond covalency apparently gains control of the physics. This observation leads us to an examination of the electronic conductivity and then semiconductor-to-metal (SC-*M*) transitions, with their associated thermodynamic manifestations in relevant liquid alloys. The thermodynamic components, as seen previously, control liquid fragility and cause fragile-to-strong transitions during cooling. We tentatively conclude that liquid-state behavior in phase-change materials is controlled by liquid-liquid (LL) and SC-*M* transitions that have become submerged below the liquidus surface. In the case of the Ge-Te binary, a crude extrapolation to GeTe stoichiometry indicates that the SC-*M* transition lies about 20% below the melting point, suggesting a parallel with the intensely researched "hidden liquid-liquid transition" in supercooled water. In the water case, superfast crystallization initiates in the high-fragility domain some 4% *above* the LL transition temperature (T_{LL}) which is located at approximately 15% below the (ambient pressure) melting point.

DOI: 10.1103/PhysRevApplied.7.034035

I. INTRODUCTION

Chalcogenide glasses comprised of chalcogen elements (S, Se, Te) covalently bonded with group-*IV* and -*V* metalloid elements with similar electronegativity such as As, Sb, Ge, and Si offer attractive optical and electronic properties for potential applications such as infrared optical fibers [1] and phase-change nonvolatile memory devices [2,3]. The knowledge of glass-transition behavior and kinetic properties of the supercooled-liquid state are crucial for applications and the understanding of this class of materials, as they are related to structural relaxations, aging, stability, processability, crystallization kinetics [4], etc. In particular, the temperature dependence of viscosity plays an important role in the nucleation and growth rates of crystals and is receiving increasing attention in the field of phase-change materials (PCMs) [5].

The concept of liquid fragility has been found useful in the discussion of the wide variety of viscosity behavior observed in glass-forming liquids [6]. A near-Arrhenius rise in viscosity with the "universal" preexponential factor 10^{-4}–10^{-5} Pa s is classified as "strong" behavior, whereas a range of non-Arrhenius to highly non-Arrhenius behavior is classified as "fragile." Fragility can be represented by the slope of the T_g-scaled Arrhenius plot (i.e., fragility plot) for viscosity η (or structural relaxation time τ) at $T = T_g$, the so-called "steepness index" or "m fragility,"

$$m = \left.\frac{d \log \eta}{d(T_g/T)}\right|_{T=T_g}, \tag{1}$$

where T_g is defined as the temperature where the viscosity increases to the value $\eta = 10^{12}$ Pa s associated with the rigid behavior [6]. Alternatively, and more common, T_g can be determined by differential scanning calorimetry (DSC), as the onset temperature for the jump in heat capacity which occurs as the liquid degrees of freedom are accessed during a "standard DSC scan" [i.e., heating at 20 K min^{-1} after vitrification at 20 K min^{-1} ($q_h = q_c = 20$ K min^{-1})]. This glass transition corresponds to the temperature at which the liquid enthalpy relaxation time reaches 100 s [6]. The two definitions are *not* always the same, as in the case of fragile liquids, the viscosity at T_g tends to be less than 10^{12} Pa s (see Fig. 1 of Ref. [7]). The m values range from 16 (perfect Arrhenius [8–10] or strong) to $m \approx 170$ for the most fragile liquids [8,11] and 200 if polymers are included.

---

[*] Author to whom all correspondence should be addressed.
austenangell@gmail.com

The determination of fragility usually requires a stable supercooled-liquid region in which the viscosity or structural relaxation times can be measured as a function of the temperature [12,13]. However, for poor glass formers, such as phase-change materials $Ge_2Sb_2Te_5$ (GST225), $Ge_1Sb_2Te_4$ (GST124), and $Ag_4In_3Sb_{67}Te_{26}$ (AIST), the glass transition and supercooled-liquid regime are difficult to probe directly, as crystallization occurs on very short time scales and preempts the T_g [14,15]. Thus, indirect methods that employ related quantities such as crystal growth rates have been used to derive the viscosity. For example, Orava *et al.* [4] studied the crystallization kinetics using nanocalorimetry with extremely high heating rates and estimated the fragility of GST225 to be high, $m \approx 90$. Salinga *et al.* [5] measured the crystal-growth velocity of AIST using time-resolved laser reflectivity experiments and derived an extremely high fragility of $m = 128$, while Zalden *et al.* [16] observing crystal growth after femtosecond-pulse optical excitation reported $m = 104$ close to T_m for the same composition. Greer and co-workers [17] suggest a broad crossover from $m = 37$ to $m = 74$ in the same liquid over a wider temperature range. High fragilities near the melting point can generally be expected from the Johnson *et al.* [18] and Greer and co-workers [19] methods based on the Turnbull parameter and the crystallization time at the nose of the time-temperature-transformation (TTT) curve.

On the other hand, there are “good” chalcogenide glass formers such as Ge-As-Se and Ge-As-S that are characterized by low-to-intermediate fragilities [20–22] ($m = 27$–65). A minimum fragility has been observed at an average bond-coordination number (or bond density) $\langle r \rangle$ higher than the rigidity percolation threshold at $\langle r \rangle = 2.4$ [21,22]. Recently, the fragility of $Ge_{15}Te_{85}$ near T_g has been determined to be relatively strong compared to its high-temperature fragile liquid state [23]. A fragile-to-strong liquid transition was revealed by the Adam-Gibbs equation [24] fitting of viscosity data [23]. It appears that the fragility of chalcogenide liquids can vary over a broad range from as strong as silica [8] ($m = 20$) to as fragile as the simple ionic glass former calcium potassium nitrate CKN ($m = 93$ [8]). However, the origin of such diverse liquid dynamics in this group–*IV-V-VI* class of materials remains unclear, and systematic studies are desirable.

The Ge-As-Te alloys have composition ranges that are good glass formers [25] with supercooled-liquid regions accessible to DSC studies. They differ from Ge-As-Se and Ge-As-S only by the difference in chalcogen elements (Te, Se, S), whereas they differ from Ge-Sb-Te by having a different group-*V* metalloid. In this regard, Ge-As-Te is a link between the former and latter types of alloys. Understanding the analogies and difference between Ge-As-Te and the related alloys may provide insights into the origin of the diverse fragilities and glass-transition behaviors in chalcogenide glasses and help reach a better understanding of the related Ge-Sb-Te phase-change materials [26]. The urgency of understanding the underlying physics of phase-change materials in the context of technological applications should need no emphasis.

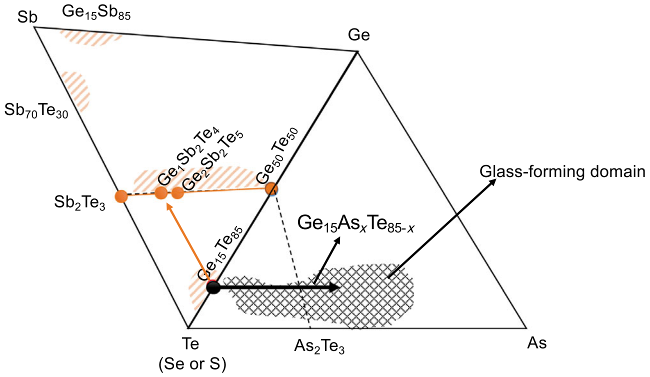

FIG. 1. Ternary phase diagrams of Ge-As-Te and Ge-Sb-Te with common Ge-Te boundary. In the Ge-As-Te ternary diagram (right triangle), the arrows indicate the composition line of $Ge_{15}As_xTe_{85-x}$ alloys studied in this work. The black shaded area is the glass-forming domain determined by the water-quenching method according to Ref. [27]. In the Ge-Sb-Te ternary diagram (left triangle), the orange dots and lines mark typical compositions of phase-change materials according to Ref. [2]. The thin orange arrow indicates the corresponding compositions in the Ge-Sb-Te system that we explore, with only limited success due to fast crystallization.

In this work, we investigate the glass transition, Turnbull parameter, and fragility using DSC on small samples that fall along the line of increasing As (or Sb) atoms replacing Te atoms (Fig. 1). The T_g and fragility behavior in Ge-(V)-(VI) $\{(V) = \text{As}$ or Sb and $(VI) = \text{S, Se, Te}\}$ alloys prove to be very different, and the differences can be rationalized in terms of the known electronic conductivities and semiconductor-metal (SC-M) transitions, thereby connecting them to the differences in metallicity of the individual alloy components. Finally, we consider how liquid fragility transitions associated with the SC-M transitions might influence the crystallization kinetics in PCMs and thereby account for the unique combination of ultrafast phase switching with large changes of electrical conductivity that characterize PCMs.

II. MATERIALS AND METHODS

Amorphous $Ge_{15}As_xTe_{85-x}$ and $Ge_{15}Sb_2Te_{83}$ samples are prepared using the Ge, As (or Sb), and Te elements with purities ranging from 99.999 to 99.9999 at. % sealed under vacuum (10^{-6} mbar) and synthesized in a rocking furnace for homogenization at 900 °C for 15 h. The melt is subsequently quenched sidewise into ice water to achieve a high cooling rate, resulting in an approximately 1-mm amorphous layer. For compositions $Ge_{15}Sb_xTe_{85-x}$ where $x > 2$, fully amorphous samples cannot be obtained using ice-water quenching or a technique with a higher quenching rate using an ice + ethanol bath due to the poor glass-forming ability caused by increased Sb concentration.

DSC studies are carried out using a TA Instruments Q1000 MDSC (TA DSC) for fragility determinations, which are carried out near T_g and a PerkinElmer Diamond DSC (PE DSC) is used to extend measurements to higher temperatures near and above 500 °C. Amorphous samples with mass about 5–15 mg are sealed in aluminum Tzero pans, and an empty aluminum pan is used as a reference. TA DSC cell calibration is carried out with standard sapphire. The temperature and enthalpy are both calibrated for each heating rate using standard indium (and zinc) prior to the measurements for TA DSC (and PE DSC). The error of the measured temperature is within 0.5 K.

The fragilities for a series of compositions along the thick black arrow of Fig. 1 are determined using the cooling-rate dependence of the fictive temperature method and also instrumentation (TA DSC) described in our previous work [21,22] on the fragility of $Ge_{15}As_xSe_{85-x}$, $Ge_{15}As_xS_{85-x}$, and also as one of the methods employed in the DSC study of $Ge_{15}Te_{85}$ [23]. The fictive temperature is defined for a given cooling rate q_c as the temperature of onset of the heat capacity jumps during upscan at the same rate, i.e., $q_h = q_c$, since the identity $T_f \approx T_g^{\text{onset}}$ is shown in earlier work [28] to hold under this protocol. More specifically, DSC scans are carried out from 25 °C through the glass transition until well above T_g to ensure the system reaches the metastable equilibrium of the supercooled-liquid state before cooling at the next q_c for the next run (for cases where crystallization at $T > T_g$ is unlikely). T_g^{onset} is determined by the usual tangent construction illustrated in the lowest curve of Fig. 2.

Figure 2 shows a series of scans for T_f determinations at different q values ranging from 3 to 30 K min^{-1} for a single composition ($Ge_{15}Sb_2Te_{83}$). For the poorer glass formers (e.g., Fig. 2), each scan is obtained with a fresh sample as a precaution against any crystallization that might occur during the short exposure to $T > T_g$. A series of scans, like that of Fig. 2, yields the value of fragility for a single composition by plots described in Sec. III.

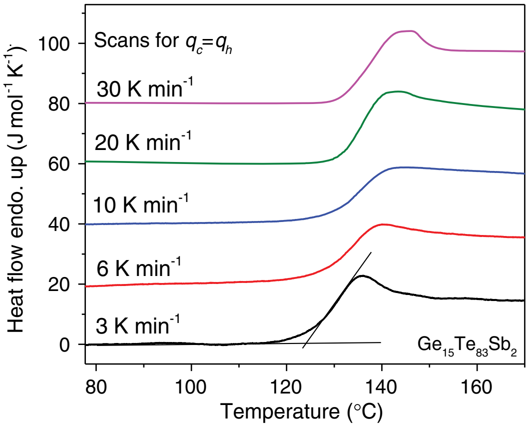

FIG. 2. DSC heat flow of $Ge_{15}Sb_2Te_{83}$ measured upon heating at various rates q_h after previous cooling (q_c) from supercooled liquid at the same rate $q_c = q_h$. The onset temperatures of the glass transitions are determined by tangent line constructions as illustrated for $q_h = 3$ K min^{-1}. The curves are vertically shifted for clarity.

III. RESULTS

Figure 3 shows the DSC heat flow during heating at 20 K min^{-1} of as-quenched amorphous samples for compositions $Ge_{15}As_xTe_{85-x}$ along the line illustrated in Fig. 1 and $Ge_{15}Sb_2Te_{83}$. Glass transitions T_g are observed as endothermic events on the DSC scans (marked by the solid triangle). With increasing temperature above T_g, the

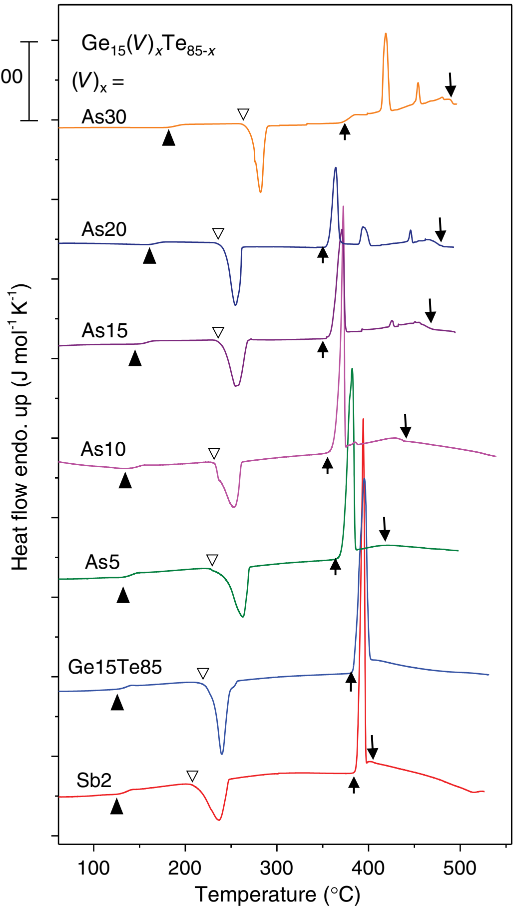

FIG. 3. DSC heat flow upon heating at 20 K min^{-1} for as-quenched samples of $Ge_{15}As_xTe_{85-x}$ and $Ge_{15}Sb_2Te_{83}$. Solid and open triangles indicate the glass-transition temperatures T_g and crystallization onset temperature T_x, respectively. The arrows point to the onset (T_e) and the end (T_L) of melting. The composition As30 apparently belongs to a different phase field. The excess heat flow for the binary (starting) composition $Ge_{15}Te_{85}$ and Sb_2 seen on the high-temperature side of the eutectic temperatures is due to the residuum of the liquid-state C_p anomaly, which is the focus of our previous article [23]. The composition line under study appears to be closely following a eutectic valley from $Ge_{15}Te_{85}$ down to a ternary eutectic near 20% As (in Fig. 1).

TABLE I. Summary of T_g, T_x, and T_L of as-quenched samples measured at 20 K min^{-1}. The activation energy E_a at T_g and the fragility m are determined using DSC methods. ΔT_{x-g} are average values from three measurements for as-quenched samples. The enthalpy of crystallization ΔH_x and enthalpy of fusion ΔH_m are determined by integrating exothermic crystallization and endothermic melting peak areas, respectively. Estimated uncertainties are included or implied by significant figures.

	T_g (K)	T_x (K)	T_L (K)	E_a (kJ mol^{-1})	Fragility m	ΔT_{x-g} (K)	t_{r_g}	ΔH_x (kJ mol^{-1})	ΔH_m (kJ mol^{-1})
$Ge_{15}As_{30}Te_{55}$	454.0	538	766	261 + 12	30 ± 3	84	0.593	4.3	7.0
$Ge_{15}As_{20}Te_{65}$	433.9	510	756	227 ± 8	27 ± 1	76	0.574	4.4	7.2
$Ge_{15}As_{15}Te_{70}$	424.5	505	743	229 ± 15	28 ± 2	81	0.571	4.9	9.7
$Ge_{15}As_{10}Te_{75}$	411.0	505	714	277 ± 14	35 ± 2	94	0.574	5.2	9.5
$Ge_{15}As_5Te_{80}$	406.3	498	723	324 ± 26	41.5 ± 3	93	0.562	5.6	11.4
$Ge_{15}Te_{85}$	403.1	475	658^{a,b}	380 + 28	49^b±3	89	0.613	5.9	10.6
$Ge_{15}Sb_2Te_{83}$	403.7	482	679	394 ± 21	51 ± 3	84	0.595	5.1	10.2

[a] Eutectic temperature.
[b] Ref. [23].

supercooled liquids crystallized (indicated by exothermic peaks; T_x marks the onset of crystallization), followed by endothermic peaks of melting that occur over a range of temperatures [the arrows point to the onset T_e and liquidus T_L temperatures]. Table I lists the values of these transition temperatures, enthalpies of fusion ΔH_m, and of crystallization ΔH_x derived from integrations of heat-flow peaks. Figure 4(a) shows that T_g of $Ge_{15}As_xTe_{85-x}$ increases with increasing As concentration, whereas T_e displays weak changes as the melting processes may involve the mixtures of different metastable phases formed during crystallization upon heating. T_L becomes higher as As atoms replace Te atoms in the alloys. Figure 4(b) shows the Turnbull parameter [29], the reduced glass temperature $t_{r_g} = T_g/T_L$, which is commonly used as an indicator of the thermodynamic driving force for crystallization, and the parameter $\Delta T_{x-g} = T_x - T_g$. The latter parameter is a measure of the width of the supercooled region that is accessible to experiment.

Next, we characterize the temperature dependence of structural relaxation times (i.e., fragility) near the glass transition. The DSC scans are carried out for a series of cooling and heating rates $q = q_h = q_c$ throughout the glass transition from room temperature to well above T_g for each composition using the procedures described in Sec. II. The obtained fictive temperatures T_f and corresponding heating (cooling) rates q for $Ge_{15}As_xTe_{85-x}$ and $Ge_{15}Sb_2Te_{83}$ are plotted in Arrhenius form in Fig. 5. From the commonly used plot of $\ln(q)$ vs $1/T_f$, the activation energy E_a near T_g can be determined by calculating the slope of a linear fit, since the slope is equal to $-E_a/R$. The E_a is related to fragility by $m = E_a/(2.303RT_g)$ [8], where T_g is the glass-transition temperature measured using a standard DSC scan

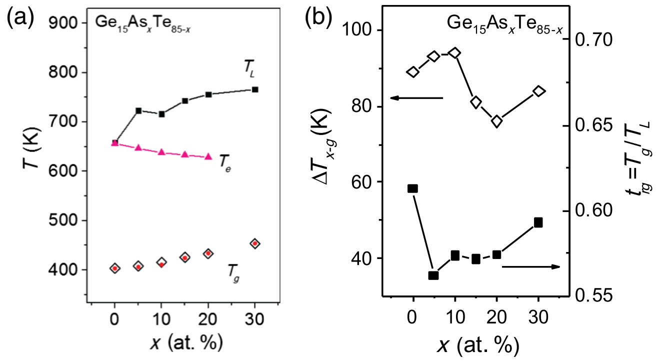

FIG. 4. (a) Glass transition T_g, melting onset (or eutectic) T_e, and liquidus T_L temperatures of $Ge_{15}As_xTe_{85-x}$ as a function of x values. The open diamonds represent T_g for as-quenched glasses measured at 20 K min^{-1}, while dots (inside diamonds) are standard T_g values under the constraint $q_h = q_c = 20$ K min^{-1}. (b) The Turnbull parameter t_{rg} (solid squares) and the width of the supercooled region ΔT_{x-g} (open diamonds). Uncertainties on the individual points are comparable with the symbol sizes.

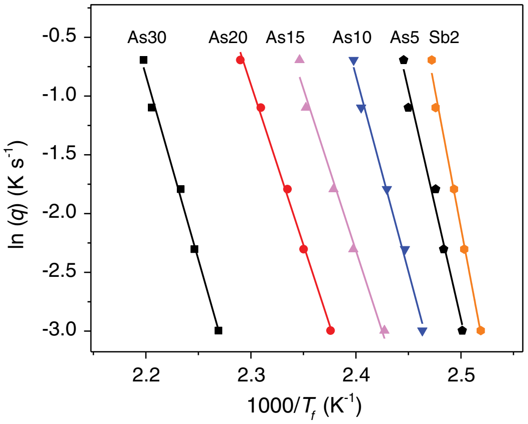

FIG. 5. The natural logarithm of scanning rate $\ln(q)$, where $q = q_h = q_c$ holds, is plotted against $1/T_f$ for $Ge_{15}As_xTe_{85-x}$ (x = 30, 20, 15, 10, 5) and $Ge_{15}Sb_2Te_{83}$. The slope of the fitted line is equal to $-E_a/R$, which is related to fragility by $m = E_a/(2.303RT_g)$, where T_g is the glass-transition temperature measured under a standard DSC scan, $q_h = q_c = 20$ K min^{-1}. Note that the same m values can be also obtained by constructing a $\ln(q)/q_s$ vs T_f^s/T_f plot (see details in Refs. [23,30]).

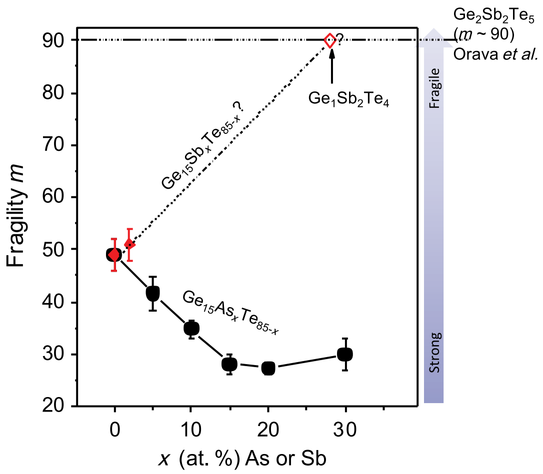

FIG. 6. The fragility m of $Ge_{15}As_xTe_{85-x}$ (solid circles) liquids as a function of x in at. % As. m ranges from intermediate to strong with increasing As content. For $Ge_{15}Sb_xTe_{85-x}$, fragility data are only available for $x = 2$ (solid diamonds). The open diamond represents the fragility $m \sim 90$ for $x = 28$ (approximately GST124; see text for details) by assuming that GST124 has a similar fragility to that of GST225 ($m \sim 90$) estimated by Orava *et al.* [4].

(i.e., upscan at 20 K min^{-1} after cooling at the same rate, $q_h = q_c = 20$ K min^{-1}). T_g defined this way corresponds to the temperature at which the structural relaxation time $\tau \sim 100$ s [30]. The results of E_a and the fragility m are summarized in Table I. As shown in Fig. 6, the fragility of $Ge_{15}As_xTe_{85-x}$ is initially lowered by a small amount of As and reaches the lowest m value 27 at around $x = 20$; i.e., the strongest liquid behavior is observed at $Ge_{15}As_{20}Te_{65}$. With further increase of As concentration, the system tends back to higher fragilities. Such a fragility behavior resembles that of $Ge_{15}As_xSe_{85-x}$ and $Ge_{15}As_xS_{85-x}$ [21,22] and exhibits almost the same $\langle r \rangle$- and As atomic percent dependence.

By striking contrast, the replacement of As by Sb as the third component at the same constant Ge causes m to change in the opposite direction. It is unfortunate that fast crystallization excludes the exploration of this effect beyond the composition $Ge_{15}Sb_2Te_{83}$. More Sb-rich compositions are found always to be contaminated by crystalline material. While this is certainly consistent with the proposed high fragilities in the Sb-containing ternaries, our composition range is too small to serve as a confirmation. The dotted line extrapolating our finding to the domain of the PCM GST124 is barely scientific. However, if we assume that GST124 has a fragility similar to the value $m \approx 90$ estimated for the neighboring GST225 from crystallization kinetics [4], then GST124 (which is approximately $Ge_{15}Sb_xTe_{85-x}$ with $x = 28$) can be represented by the open diamond in Fig. 6, where it supports the dramatic difference between the As-based and Sb-based systems with respect to fragility behavior. Such a contrast in the effect of the group-V element on the physical behavior is certainly eye catching, and its physical origin demands an explanation. This is taken up in Sec. V after some consideration of the glass-transition temperatures themselves, in relation to chalcogenide component.

IV. DISCUSSION

The increase of T_g as cross-linking elements like Ge and As are added to the chalcogen selenium is a familiar phenomenon [20,31,32]. Not so well recognized is the more rapid increase in the case of the chalcogen sulfur [22] and, of special importance to us, the much *less* rapid increase when the chalcogen is Te. The relations are summarized in Fig. 7. It has been common, following Phillips [36,37] and Phillips and Thorpe [38], to use the bond-coordination number or bond density $\langle r \rangle$ as the correlating composition variable, although more recent studies [21] suggest it is an oversimplification. $\langle r \rangle$ is obtained by summing the products of bond number (from the $8 - N$ rule) and atom fraction in the sample. Thus, for a Ge-As-Te glass with 15 at. % Ge, it is given by $\langle r \rangle = [4 \times 15 + 3x + 2 \times (85\text{-}x)]/100$, where x is the

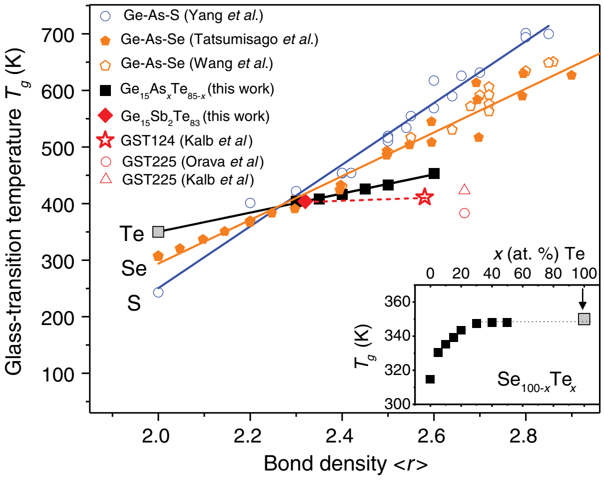

FIG. 7. Glass-transition temperature T_g as a function of bond density $\langle r \rangle$ for $Ge_{15}As_xTe_{85-x}$ (this work), Ge-As-Se (Tatsumisago *et al.* [20] and Wang *et al.* [21]), and Ge-As-S (Yang *et al.* [22]). The linear variation is a good approximation up to $\langle r \rangle$ values of 2.4. Beyond $\langle r \rangle = 2.4$, composition-specific effects are found [20,22], causing the spread of data points. More scattered data for Ge-As-Te glasses from early work by Savage [33] and additional data from Lucas *et al.* [34] (not shown) support the present findings at slightly lower T_g values. For Te- based glasses with $\langle r \rangle$ increased by Sb instead of As (thus, entering the fast-crystallizing PCM domain), the behavior becomes uncertain and confusing. Some estimates imply weak positive dependence of T_g on $\langle r \rangle$, while others require decreases, as we discuss in the text. Inset: The glass-transition temperature of $Se_{100-x}Te_x$ alloys [35]. The gray square is the extrapolated $T_g = 350$ K of pure Te and is consistent with the value extrapolated from the data in the main panel.

atomic percentage of As in the sample. We notice in Fig. 7 that while the increase in T_g is rapid when the chalcogen that is being crosslinked by the As or Ge is S or Se, when it comes to Te, the increase in T_g is small. Finally, when As is replaced by Sb, as in the PCMs, the T_g increase, to the extent that it can be measured or estimated, virtually disappears for $\langle r \rangle$ greater than 2.3, which is the crossover value, where all systems have T_g of 400 K. For instance, Kalb *et al.* [15], studying sputtered compositions that are annealed before scanning to remove the quenched-in high-temperature structure, find $T_g = 411$ K for GST124 (with $\langle r \rangle = 2.57$) and 430 K for GST225 ($\langle r \rangle = 2.67$). On the other hand, Orava *et al.* [4] found reasons for using the much lower value of $T_g = 383$ K for GST225. The confused state of debate is reminiscent of the notorious case of vitreous water, where hyperquenched glass studies also indicate high T_g values [39–41], while work on glasses formed by other routes [42,43] or extrapolated from binary solutions [44,45] yield much lower values. In any case, it appears that covalency of interaction and the related average bond density can no longer be the dominant consideration for GST glasses.

Indeed, when the electronic conductivity of these materials is examined, it becomes clear that the concept of electron localization in a covalent bond is becoming very fuzzy. Figure 8 adapted from the works of Alekseev *et al.* [46], Tsuchiya-Saitoh [61], and Nagels *et al.* [50] presents electronic conductivity data in Arrhenius form for a variety of chalcogenides as they pass from low-temperature semiconducting states to high-temperature "weak-metal" states [at the Mott minimum metallic conductivity of approximately $10^3\ \Omega^{-1}\,\mathrm{cm}^{-1}$ through a maximum in the apparent activation energy [Fig. 8(a)]]. Figure 8(b) shows how this SC-*M* transition at 1280 K for the case of As_2Se_3 occurs at the same temperature as the closing of the optical band gap (1250 K), which is also the temperature of a thermodynamic anomaly in the density [density minimum and maximum with thermal expansion coefficient extremum $\alpha(\mathrm{min})$ at approximately 1280 K] [$\alpha = 1/V(\partial V/\partial T)_p$]. The transition occurs far above the melting point of 641 K [51] for As_2Se_3, but when Se is replaced by Te, the density anomaly with extremum $\alpha(\mathrm{min})$ occurs at 780 K, much closer to T_m (640 K) [47]. Finally, when the more metallic bismuth replaces arsenic, the liquid Bi_2Te_3 is already metallic at its 857-K [52] melting point [see Fig. 8(c)], meaning the SC-*M* transition is pushed below the melting point and can no longer be observed due to fast crystallization. If the SC-*M* transition is sharp enough, then the accompanying heat-capacity change will be sharp, and according to Adam-Gibbs theory, a fragile-to-strong transition (in which the viscosity changes more or less suddenly by some orders of magnitude) will occur during cooling [23]. We discuss the importance of such a viscosity change further below.

Considering lower temperatures in the glassy state, one can see how dramatically the glassy conductivity responds to the change in metallicity of the components [50]. Figure 8(c) shows the effect of doping $GeSe_{3.5}$ glasses

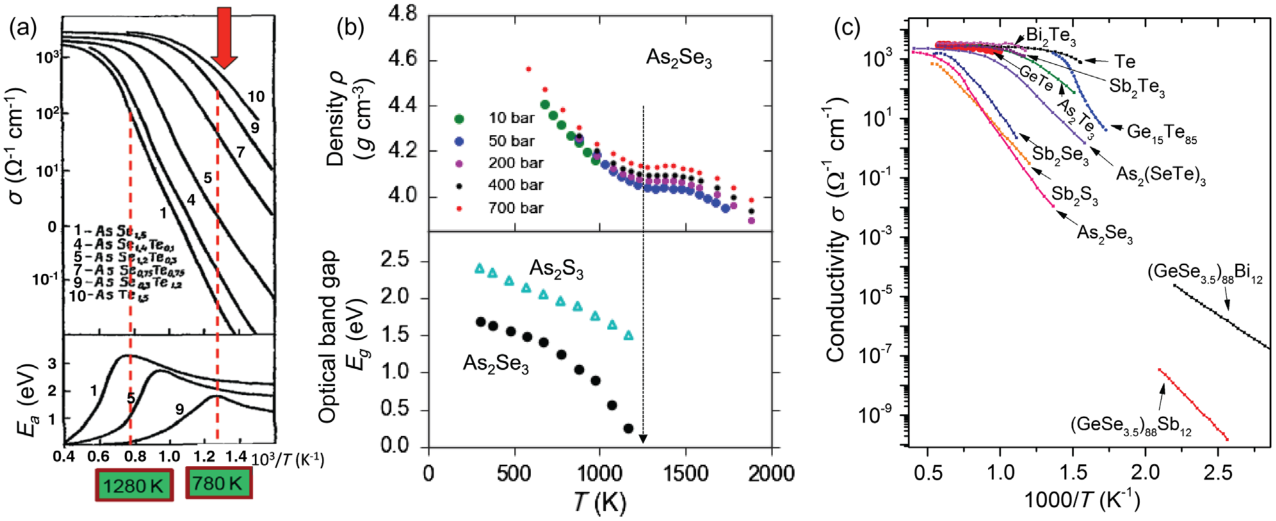

FIG. 8. (a) Electronic conductivity of liquid As_2Se_3-As_2Te_3 alloys (upper panel) and the apparent activation energy E_a for conductivity (lower panel) (adapted from Ref. [46]). The dashed lines mark the temperatures of the maximum E_a, i.e., the SC-*M* transition temperature $T_{\mathrm{SC}\text{-}M}$. The arrow points to the temperature $T(C_p^{\max})$ of the heat capacity anomaly of As_2Te_3 (780 K) [47]. (b) Upper panel: Densities of liquid As_2Se_3 at various pressures showing density anomalies. The phase-transition temperature is where the minimum in $\alpha(T)$ occurs. Lower panel: Optical band gap of liquid As_2Se_3 closes at approximately 1250 K and that of As_2S_3 closes at a higher temperature. Data taken from Refs. [48,49]. (c) Electronic conductivities for a variety of liquid chalcogenide and two glasses (data reproduced from Refs. [46,50,61]). Note that the conductivities approach a plateau of the order of magnitude approximately $10^3\ \Omega^{-1}\,\mathrm{cm}^{-1}$ (the Mott minimum metallic conductivity) by a SC-*M* transition.

alternatively with just 12 at. % Sb vs 12 at. % Bi in the system $(\mathrm{GeSe}_{3.5})_{88}\mathrm{Sb}_{12}$ can cause a change of some 3 orders of magnitude.

As the band gap closes, an increasing fraction of the valence electrons involved in the covalent bonds are promoted into the conduction band or into the more diffuse tail states of Mott-Anderson theory [53] where they are delocalized, and the constraint counting involved in the assessment of average bond density $\langle r \rangle$ becomes increasingly irrelevant to the physics of the system. For this reason, we expect that the dependence of T_g on $\langle r \rangle$ should become weaker to vanishing. The latter behavior is the case of Ge-Sb-Te phase-change alloys.

The decreasing relevance of the bond density is also reflected in the loss of glass-forming ability. For instance, in the case of the composition $\mathrm{As_2Se_3}$ for which $\langle r \rangle = 2.4$ (the "magic" bond density), the "good glass-former" characteristics were used as support for the constraint-counting theory [36]. However, when there is total replacement of Se by Te to give the more metallic $\mathrm{As_2Te_3}$, the $\langle r \rangle$ value remains the same but the glass-forming ability is lost. In that case, the SC-M transition at 780 K closely approaches the melting point of 640 K, and it is clear that if the As is replaced by the next lower in group V, Sb, the temperature of the SC-M transition will fall below the melting point. Indeed, as seen in Fig. 8(c), $\mathrm{Sb_2Te_3}$ is metallic at its melting point. The problem is then to decide how far below the melting point the transition actually would occur, what could be the physical consequences, and finally to what extent a substantial Ge component in GST PCMs would modify the effect of Sb replacement of As in the series just discussed. A study of the LL transition with increasing Sb in the binary system $\mathrm{As_2Te_3}$-$\mathrm{Sb_2Te_3}$ would be helpful, but it does not appear to have been made. We predict that systematic changes in the temperature of the SC-M transition would be observed as the Sb content increases and that an extrapolation could be made to locate the sub-T_m value for $\mathrm{Sb_2Te_3}$.

At this point, it is profitable to consider the phenomenologically related case of the "most anomalous" liquid, viz., water and particularly supercooled water, for which a strict limit on supercooling is found at a temperature that is some 15% below its melting point. This limit on supercooling is apparently a direct consequence of the structural fluctuations associated with an impending LL phase transition. The phenomenology of "hidden" LL phase transitions and their relation to fast crystallization in supercooled water has been the subject of exhaustive studies both by experiment and computer simulation [54], to which brief reference is made in our preceding paper [23]. In the water case, the response functions heat capacity, compressibility, and expansivity of water all show highly anomalous behavior with an apparent common divergence temperature just below the sharply defined homogeneous nucleation temperature (which can be measured for aqueous systems using small sample techniques). Furthermore, the liquid immediately above the supercooling limit is extremely fragile in character. To date, it has still not been possible to reach clear conclusions on whether the transition in the laboratory substance $\mathrm{H_2O}$ at ambient pressure is first order as in liquid Si [55] or higher order as in $\mathrm{As_2Te_3}$ [47]. To add plausibility to this parallel, we note the recent structural studies on GST124 by Clark and co-workers [56] that not only lead to the observation of high-pressure amorphization of the crystalline form (analogous to the pressure-induced amorphization of the ambient pressure stable polymorph ice Ih by Mishima [57]) but give evidence of a reversible polyamorphic phase transition when starting with the sputtered glassy form comparable to the famous studies of Mishima for glassy water [58].

If we translate these observations to the liquid GST case (specifically, GST225), we can begin to understand the reason why crystallization studies have yielded the conclusion that the crystallizing liquid is very fragile ($m \approx 90$ [4]). It should be because they are being studied on the high-temperature side of the LL (now also SC-M) transition. To gain some additional support for this notion, we can plot the temperatures of the heat-capacity maxima (i.e., the SC-M transition temperatures) on the phase diagram for Ge-Te and extrapolate to the PCM composition GeTe. This is shown in Fig. 9, where it is seen crudely to locate the SC-M transition at approximately 800 K, some 20% below the melting point (cf. the 15% for water noted above).

Finally, to support this thesis, we note the work of Zalden *et al.* [63] on the $\mathrm{Ge_{15}Sb_{85}}$ alloy, another PCM that is used in phase-change memory devices. Using short laser pulses, they induced fast melt-quench cycles in $\mathrm{Ge_{15}Sb_{85}}$ and

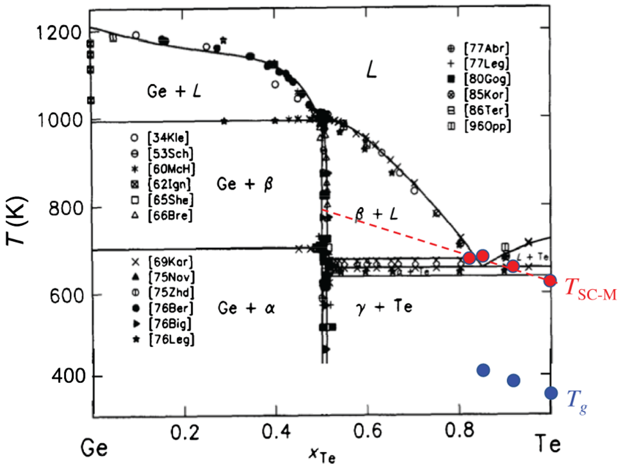

FIG. 9. Preliminary estimate of the SC-M transition temperature $T_{\mathrm{SC}\text{-}M}$ in a phase-change material GeTe on the binary Ge-Te phase diagram [59]. An extrapolation to approximately 800 K for GeTe is based on the temperatures of liquid $C_p(\max)$ (red solid circles) [60,61]. T_g are represented by solid blue circles ($\mathrm{Ge_{15}Te_{85}}$ [23], $\mathrm{Ge_{10}Te_{90}}$ [62], and Te, 350 K from Fig. 7).

employed ultrafast x-ray scattering to probe the structural changes of the undercooled state. A structural transition was observed just before crystallization set in, although it was difficult to determine the exact temperature of the transition. Supporting this observation and our arguments is also a very recent *ab initio* calculation on GST225 that reported a pseudogap at the Fermi energy which opened with decreasing temperature, suggesting a SC-*M* transition will occur at a somewhat lower temperature below 852 K [64].

Thus, the connection between submerged LL phase transitions, fragile liquid behavior, and fast crystallization kinetics gains some credibility without being established. From water phenomenology, the LL transition should always occur below the temperature of the density maximum. A more detailed investigation of this phenomenology and an indirect means of assessing the relation between SC-*M* and melting transition temperatures is the subject of a broad overview paper to be published separately.

A. Synopsis and technological relevance

For phase-change memory applications that greatly improve on the original and most common “flash” memory devices, PCMs must possess a unique combination of properties, namely, extremely fast phase switching (time scale of nanoseconds) at high temperature and a high stability of amorphous and crystalline phases at room temperature, as well as a strong optical and electrical contrast between the two phases. The strong contrast owes its existence to the metal-semiconductor transition, which we particularly note is closely linked to structural fluctuations that are jointly the source of thermodynamic anomalies and enhanced nucleation rates (as has been so well studied in supercooled water). If these enhanced nucleation rates can be induced to occur at an optimum supercooling, (i.e., optimum $T_{\text{SC-}M}/T_m < 1$), they should facilitate the crystallization process and greatly speed up the phase switching, thus, explaining how nanosecond switching behavior is possible in PCMs. But when the cooling rate is increased sufficiently to avoid crystallization, the fragile-to-strong liquid transition that is the companion to the M-SC transition will quickly lock-in the amorphous configuration in a kinetically stable vitreous state until a new heat pulse raises it back to the fast crystallization domain.

The applied technology problem then is to ensure that, on the one hand, $T_{\text{SC-}M}/T_m$ is low enough for the thermodynamic crystallization driving force G_{liq}-G_{cryst} to be sufficient to drive the process, while on the other hand, that $T_{\text{SC-}M}/T_m$ is not so low that the system becomes a viscous glass former that retains the metallic state and so shows little electrical contrast even if crystallization should occur. Accordingly, a key to the favored properties of PCMs is the “tuning” of $T_{\text{SC-}M}/T_m$ by, for instance, doping in of elements of the appropriate metallicities whose role in moving the SC-*M* transition has been discussed above.

V. CONCLUDING REMARKS

It is intriguing to find such high levels of phenomenological similarity between such seemingly different condensed phases of matter as we suggest in the foregoing discussion. However, this is not a new observation, except for the connection to PCM phenomenology. The extraordinary parallel in physical behavior between water and the element tellurium in their supercooled-liquid states was detailed in the T_m-scaled plots of volume, heat capacity, and isothermal compressibility by Kanno *et al.* [65] in 2001 and interpreted by one of us [66] as a consequence of each liquid being characterized by two different length scales—as in the Jagla model of anomalous liquids [67,68]. There are frequent references in the PCM literature to the two different Ge coordination states that might play an equivalent role.

While there are controversies associated with the fact that water and Te are most anomalous in their supercooled states [69], the LL phase transition in the starting composition for our study, $\text{Ge}_{15}\text{Te}_{85}$, has its heat capacity maximum in the thermodynamically stable domain just above the melting point (eutectic temperature) ($\text{T}_{\text{SC-}M}/\text{T}_m \approx 1.01$) and, thus, cannot be regarded as a transient Ostwald stage on the route to crystallization, as has been proposed for water [69]. This transition and this composition can then be seen to lie at the crossover between the two sorts of behaviors, i.e., at the point at which covalency loses its control of structure in favor of metallicity. Additionally, the fluctuations in structure, which accompany the transition, enhance the probability of crystal nucleation in proportion to the degree of supercooling at which they reach their maximum value. The possibility that a nearby SC-*M* transition may facilitate crystallization and speed up the phase switching implies, as we already state above, that a key parameter in the assessment of PCM phenomenology should be the temperature relative to the melting point, $T_{\text{SC-}M}/T_m$, at which the SC-*M* transition occurs. However, this reduced temperature $T_{\text{SC-}M}/T_m$ must be very difficult to observe in PCMs by direct measurement. As in the case of water, it will need to be assessed by measurements made in or near the stable-liquid domain (preferably in microscopic samples to reduce nucleation probabilities) followed by fitting to appropriate theoretical functions. It will likely remain unknown whether or not the SC-*M* transition is first order in some cases or continuous as it is in the examples of Fig. 8. *Ab initio* computer simulations will have an important role to play in clarifying the outstanding issues. The possibility of a liquid-liquid critical point playing a role was conjectured long ago [70].

ACKNOWLEDGMENTS

The authors acknowledge support from National Science Foundation research Grants No. CHE-1213265 (for CAA) and No. ECCS-1201865 (for PL). S. W. acknowledges the financial support from an Alexander von Humboldt Foundation Feodor Lynen Postdoctoral Research Fellowship.

[1] Z. Yang, T. Luo, S. Jiang, J. Geng, and P. Lucas, Single-mode low-loss optical fibers for long-wave infrared transmission, Opt. Lett. **35**, 3360 (2010).

[2] M. Wuttig and N. Yamada, Phase-change materials for rewriteable data storage, Nat. Mater. **6**, 824 (2007).

[3] B. G. Aitken and C. M. Smith, Phase Change Memory Materials, U.S. Patent No. 8,206,804 (26 June 2016).

[4] J. Orava, L. Greer, B. Gholipour, D. W. Hewak, and C. E. Smith, Characterization of supercooled liquid $Ge_2Sb_2Te_5$ and its crystallization by ultrafast-heating calorimetry, Nat. Mater. **11**, 279 (2012).

[5] M. Salinga, E. Carria, A. Kaldenbach, M. Bornhöfft, J. Benke, J. Mayer, and M. Wuttig, Measurement of crystal growth velocity in a melt-quenched phase-change material, Nat. Commun. **4**, 2371 (2013).

[6] C. A. Angell, Formation of glasses from liquids and biopolymers, Science **267**, 1924 (1995).

[7] L. M. Martinez and C. A. Angell, A thermodynamic connection to the fragility of glass-forming liquids, Nature (London) **410**, 663 (2001).

[8] R. Bohmer, K. L. Ngai, C. A. Angell, and D. J. Plazek, Nonexponential relaxations in strong and fragile glass formers, J. Chem. Phys. **99**, 4201 (1993).

[9] C. A. Angell, Relaxation in liquids, polymers and plastic crystals—Strong fragile patterns and problems, J. Non-Cryst. Solids **131–133**, 13 (1991).

[10] S. Wei, I. Gallino, R. Busch, and C. A. Angell, Glass transition with decreasing correlation length during cooling of $Fe_{50}Co_{50}$ superlattice and strong liquids, Nat. Phys. **7**, 178 (2011).

[11] L.-M. Wang, Enthalpy relaxation upon glass transition and kinetic fragility of molecular liquids, J. Phys. Chem. B **113**, 5168 (2009).

[12] R. Busch, W. Liu, and W. L. Johnson, Thermodynamics and kinetics of the $Mg_{65}Cu_{25}Y_{10}$ bulk metallic glass forming liquid, J. Appl. Phys. **83**, 4134 (1998).

[13] Z. Evenson and R. Busch, Equilibrium viscosity, enthalpy recovery and free volume relaxation in a $Zr_{44}Ti_{11}Ni_{10}Cu_{10}Be_{25}$ bulk metallic glass, Acta Mater. **59**, 4404 (2011).

[14] P. Zalden, K. S. Siegert, S. Rols, H. E. Fischer, F. Schlich, T. Hu, and M. Wuttig, Specific heat of $(GeTe)_x(Sb_2Te_3)_{1-x}$ phase-change materials: The impact of disorder and anharmonicity, Chem. Mater. **26**, 2307 (2014).

[15] J. Kalb, M. Wuttig, and F. Spaepen, Calorimetric measurements of structural relaxation and glass transition temperatures in sputtered films of amorphous Te alloys used for phase change recording, J. Mat. Res. **22**, 748 (2007).

[16] P. Zalden, A. von Hoegen, P. Landreman, M. Wuttig, and A. M. Lindenberg, How supercooled liquid phase-change materials crystallize: Snapshots after femtosecond optical excitation, Chem. Mater. **27**, 5641 (2015).

[17] J. Orava, H. Weber, I. Kaban, and A. L. Greer, Viscosity of liquid Ag-In-Sb-Te: Evidence of a fragile-to-strong crossover, J. Chem. Phys. **144**, 194503 (2016).

[18] W. L. Johnson, J. H. Na, and M. D. Demetriou, Quantifying the origin of metallic glass formation, Nat. Commun. **7**, 10313 (2016).

[19] J. Orava and A. L. Greer, Fast and slow crystal growth kinetics in glass-forming melts, J. Chem. Phys. **140**, 214504 (2014).

[20] M. Tatsumisago, B. L. Halfpap, J. L. Green, S. M. Lindsay, and C. A. Angell, Fragility of Ge-As-Se Glass-Forming Liquids in Relation to Rigidity Percolation, and the Kauzmann Paradox, Phys. Rev. Lett. **64**, 1549 (1990).

[21] T. Wang, O. Gulbiten, R. Wang, Z. Yang, A. Smith, B. Luther-Davies, and P. Lucas, Relative contribution of stoichiometry and mean coordination to the fragility of Ge-As-Se glass forming liquids, J. Phys. Chem. B **118**, 1436 (2014).

[22] Y. Yang, B. Zhang, A. Yang, Z. Yang, and P. Lucas, Structural origin of fragility in Ge-As-S glasses investigated by calorimetry and Raman spectroscopy, J. Phys. Chem. B **119**, 5096 (2015).

[23] S. Wei, P. Lucas, and C. A. Angell, Phase change alloy viscosities down to T_g using Adam-Gibbs-equation fittings to excess entropy data: A fragile-to-strong transition, J. Appl. Phys. **118**, 034903 (2015).

[24] G. Adam and J. H. Gibbs, On the temperature dependence of cooperative relaxation properties in glass-forming liquids, J. Chem. Phys. **43**, 139 (1965).

[25] P. Jóvári, P. Lucas, Z. Yang, B. Bureau, I. Kaban, B. Beuneu, and J. Bednarčik, Short-range order in Ge-As-Te glasses, J. Am. Ceram. Soc. **97**, 1625 (2014).

[26] D. Lencer, M. Salinga, B. Grabowski, T. Hickel, J. Neugebauer, and M. Wuttig, A map for phase-change materials, Nat. Mater. **7**, 972 (2008).

[27] Z. Yang and P. Lucas, Tellurium-based far-infrared transmitting glasses, J. Am. Ceram. Soc. **92**, 2920 (2009).

[28] C. A. Angell, Liquid fragility and the glass transition in water and aqueous solutions, Chem. Rev. **102**, 2627 (2002).

[29] D. Turnbull, Under what conditions can a glass be formed? Contemp. Phys. **10**, 473 (1969).

[30] L.-M. Wang, V. Velikov, and C. A. Angell, Direct determination of kinetic fragility indices of glass-forming liquids by differential scanning calorimetry: Kinetic versus thermodynamic fragilities, J. Chem. Phys. **117**, 10184 (2002).

[31] K. Tanaka, Glass transition of covalent glasses, Solid State Commun. **54**, 867 (1985).

[32] U. Senapati and A. K. Varshneya, Viscosity of chalcogenide glass-forming liquids: An anomaly in the "strong" and "fragile" classification, J. Non-Cryst. Solids **197**, 210 (1996).

[33] J. A. Savage, Glass forming region and DTA survey in the Ge-As-Te memory switching glass system, J. Mater. Sci. **6**, 964 (1971).

[34] P. Lucas, G. J. Coleman, D. C. Kaseman, Z. Yang, I. Hung, Z. Gan, and S. Sen, Structural analysis of Cu-As-Te glasses: Results from Raman and ^{65}Cu NMR spectroscopy, J. Non-Cryst. Solids **432**, 527 (2016).

[35] G. Ghosh, R. C. Sharma, D. T. Li, and Y. a. Chang, The Se-Te (selenium-tellurium) system, J. Phase Equilib. **15**, 213 (1994).

[36] J. C. Phillips, Topology of covalent non-crystalline solids I: Short-range order in chalcogenide alloys, J. Non-Cryst. Solids **34**, 153 (1979).

[37] J. C. Phillips, Topology of covalent non-crystalline solids II: Medium-range order in chalcogenide alloys and A-Si(Ge), J. Non-Cryst. Solids **43**, 37 (1981).

[38] J. C. Phillips and M. F. Thorpe, Constraint theory, vector percolation and glass formation, Solid State Commun. **53**, 699 (1985).

[39] V. Velikov, S. Borick, and C. A. Angell, The glass transition of water, based on hyperquenching experiments, Science **294**, 2335 (2001).

[40] Y. Yue and C. A. Angell, Clarifying the glass-transition behaviour of water by comparison with hyperquenched inorganic glasses, Nature (London) **427**, 717 (2004).

[41] A. Hallbrucker and E. Mayer, Calorimetric study of the vitrified liquid water to cubic ice phase transition, J. Phys. Chem. **91**, 503 (1987).

[42] K. Amann-Winkel, C. Gainaru, P. H. Handle, M. Seidl, H. Nelson, R. Böhmer, and T. Loerting, Water's second glass transition, Proc. Natl. Acad. Sci. U.S.A. **110**, 17720 (2013).

[43] A. Hallbrucker, E. Mayer, and G. P. Johari, Glass-liquid transition and the enthalpy of devitrification of annealed vapor-deposited amorphous solid water: A comparison with hyperquenched glassy water, J. Phys. Chem. **93**, 4986 (1989).

[44] D. H. Rasmussen and A. P. MacKenzie, Glass transition in amorphous water. Application of the measurements to problems arising in cryobiology, J. Phys. Chem. **75**, 967 (1971).

[45] D. R. MacFarlane and C. A. Angell, Glass transition for amorphous solid water, J. Phys. Chem. **88**, 759 (1984).

[46] V. A. Alekseev, A. A. Andreev, and M. V. Sadovskii, Semiconductor-metal transition in liquid semiconductors, Sov. Phys. Usp. **23**, 551 (1980).

[47] Y. S. Tveryanovich, V. M. Ushakov, and A. Tverjanovich, Heat of structural transformation at the semiconductor-metal transition in As_2Te_3 liquid, J. Non-Cryst. Solids **197**, 235 (1996).

[48] S. Hosokawa, Y. Sakaguchi, and K. Tamura, X-ray diffraction measurements for liquid As_2Se_3 up to the semiconductor-metal transition region, J. Non-Cryst. Solids **150**, 35 (1992).

[49] S. Hosokawa, Y. Sakaguchi, H. Hiasa, and K. Tamura, Optical absorption spectra of liquid As_2S_3 and As_2Se_3 over a wide temperature range, J. Phys. Condens. Matter **3**, 6673 (1991).

[50] P. Nagels, M. Rotti, and S. Vikhrov, Doping of chalcogenide glasses in the Ge-Se and Ge-Te systems, J. Phys. (Paris), Colloq. **42**, C4-907 (1981).

[51] M. B. Myers and E. J. Felty, Heats of fusion of the $A_2^{\mathrm{V}}B_3^{\mathrm{VI}}$ compounds As_2S_3, As_2Se_3, As_2Te_3, and Sb_2S_3, J. Electrochem. Soc. **117**, 818 (1970).

[52] B. Predel, in *B-Ba-C-Zr*, edited by O. Madelung (Springer, Berlin 1992), pp. 1–7.

[53] N. F. Mott, *Nobel Lecture, Physics 1971-1980*, edited by S. Lundqvist (World Scientific Publishing Co., Singapore, 1992).

[54] P. Gallo, K. Amann-Winkel, C. A. Angell, M. A. Anisimov, F. Caupin, C. Chakravarty, E. Lascaris, T. Loerting, A. Z. Panagiotopoulos, J. Russo, J. A. Sellberg, H. E. Stanley, H. Tanaka, C. Vega, L. Xu, and L. G. M. Pettersson, Water: A tale of two liquids, Chem. Rev. **116**, 7463 (2016).

[55] S. Sastry and C. A. Angell, Liquid-liquid phase transition in supercooled silicon, Nat. Mater. **2**, 739 (2003).

[56] B. Kalkan, S. Sen, J.-Y. Cho, Y.-C. Joo, and S. M. Clark, Observation of polyamorphism in the phase change alloy $Ge_1Sb_2Te_4$, Appl. Phys. Lett. **101**, 151906 (2012).

[57] O. Mishima, Relationship between melting and amorphization of ice, Nature (London) **384**, 546 (1996).

[58] O. Mishima, Reversible first-order transition between two H_2O amorphs at ~0.2 GPa and ~135 K, J. Chem. Phys. **100**, 5910 (1994).

[59] A. Schlieper, Y. Feutelais, S. G. Fries, B. Legendre, and R. Blachnik, Thermodynamic evaluation of the germanium-tellurium system, CALPHAD: Comput. Coupling Phase Diagrams Thermochem. **23**, 1 (1999).

[60] Y. Tsuchiya, Thermodynamics of the structural changes in the liquid Ge-Te system around the Te-rich eutectic composition, J. Non-Cryst. Solids **312–314**, 212 (2002).

[61] Y. Tsuchiya and H. Saitoh, Semiconductor-metal transition induced by the structural transition in liquid $Ge_{15}Te_{85}$, J. Phys. Soc. Jpn. **62**, 1272 (1993).

[62] I. Kaban, E. Dost, and W. Hoyer, Thermodynamic and structural investigations of heat-treated amorphous Ge-Te alloys, J. Alloys Compd. **379**, 166 (2004).

[63] P. Zalden, F. Quirin, J. Siegel, M. Shu, M. Chollet *et al.*, "Crystallization dynamics of phase-change materials resolved by ultrafast x-ray scattering," in *Proceedings of DESY Photon Science and European XFEL Users' Meeting*, 2016.

[64] M. Schumacher, H. Weber, P. Jóvári, Y. Tsuchiya, T. G. Youngs, I. Kaban, and Riccardo Mazzarello, Structural, electronic and kinetic properties of the phase-change material $Ge_2Sb_2Te_5$ in the liquid state, Sci. Rep. **6**, 27434 (2016).

[65] H. Kanno, H. Yokoyama, and Y. Yoshimura, A new interpretation of anomalous properties of water based on Stillinger's postulate, J. Phys. Chem. B **105**, 2019 (2001).

[66] C. A. Angell, Thermodynamics: Highs and lows in the density of water, Nat. Nanotechnol. **2**, 396 (2007).

[67] E. A. Jagla, Phase behavior of a system of particles with core collapse, Phys. Rev. E **58**, 1478 (1998).

[68] E. A. Jagla, Core-softened potentials and the anomalous properties of water, J. Chem. Phys. **111**, 8980 (1999).

[69] D. T. Limmer and D. Chandler, The putative liquid-liquid transition is a liquid-solid transition in atomistic models of water. II, J. Chem. Phys. **138**, 214504 (2013).

[70] C. A. Angell, in *Physics and Applications of Disordered Materials*, edited by M. Popescu (INOE, Bucharest, 2002), Chap. 1, pp. 1–18.